Chapter 27

Connections Couple Computations Across Columns

Detailed examination of superficial-layer pyramidal neuron; long-range horizontal connections; optical imaging; Gestalt good continuation; co-linear facilitation; redundancy of representation in columns; monocular occlusion clues; first computational results

27.1 Introduction

We recall the cartoon for organizing superficial V1 into a series of orientation columns; and we recall that this implies covering the visual array with receptive fields that overlap in position and vary in orientation; see Fig. 27.1. Our focus in this lecture is: are the computations in columns independent, as we have been thinking about them, or is there some basic architectural dependency among the cells comprising a column?

27.2 Computations and Columns

Given the possibility of computations running between columns, we now turn to the question of what this might be. The natural place to start is to consider the distribution of compations "along" the column.

27.2.1 Redundancy Among Local Responses

The first question to consider is why the visual system employs so many redundant representations for orientation. Recall from the development of gradient-based edge detectors (Lecture XXXX) that two orthogonal filters suffice. This was used, for example, in the Sobel edge detector. However, a first interpretation of the multiple

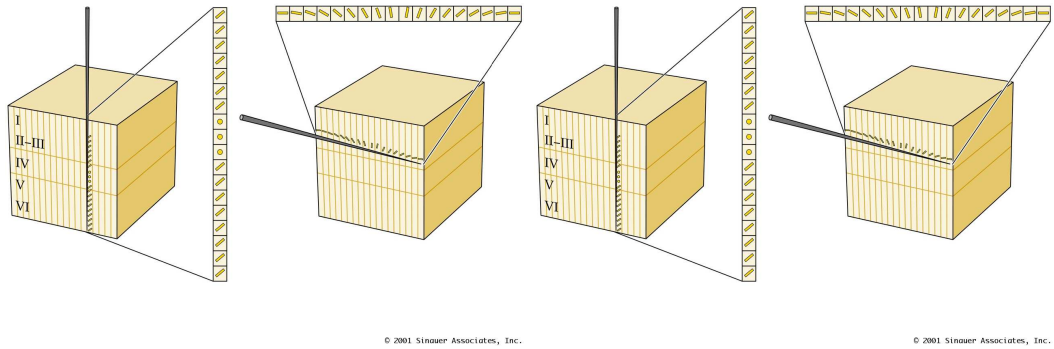

Figure 27.1: The backbone architecture for superficial layers of V1. (left) Recalling an orientation column via tangential penetration (cf. Chapter XX). (right) Rearrangement of the orientation columns to illustrate their layout geometry. At each retinotopic position are collections of cells with receptive field centers roughly aligned but spanning all orientations (and other receptive field properties)
.

cells in the columnar architecture suggests that, if they are all evaluated against the image, the result is a thickened, very messy expansion of responses around the correct, or desired one; see Fig. 27.2. (We had already seen a version of this thickening when considering the use of regularized derivatives to reduce noise.) Now the "thickening" is happening in the orientation dimension as well as the spatial dimension.

The intermediate responses in particular are an issue, because they may be the result of operators that are almost at the correct orientation, or they may be the result of noise. How might these two cases be distinguished? How might some of the incorrect responses be removed? Some use of context is necessary.

27.2.2 Context Beyond the Classical Receptive Field

Given the profusion of receptive field responses, we must question whether they are all independent from one another.

An early, classical experiment[1] was performed using slightly more complicated stimuli than simple gratings – a grating within the classical receptive field surrounded by a grating of perhaps a different orientation; see Fig.27.3. This could provide information about whether there was any interaction between orientations within a small neighborhood.

[1]Lateral inhibition between orientation detectors in the cat's visual cortex Colin Blakemore and Elisabeth A. Tobin, Experimental Brain Research, Volume 15, Number 4 / September, 1972

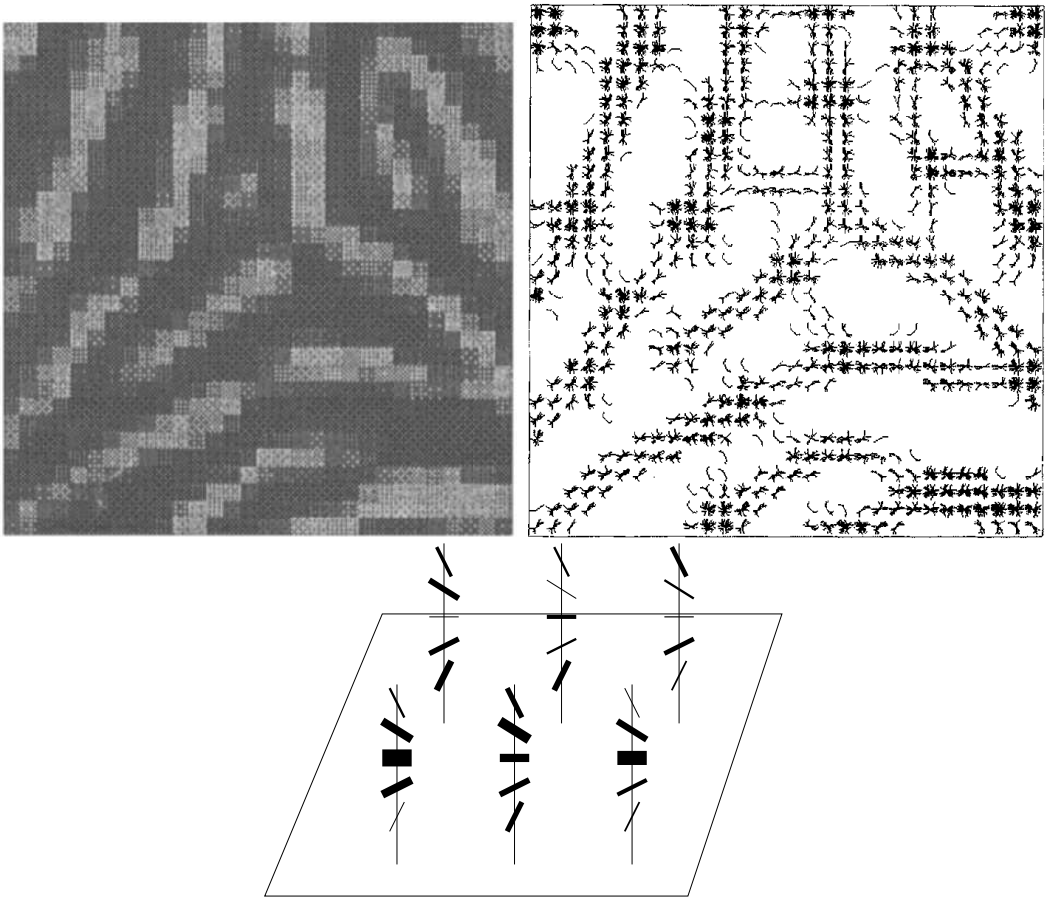

Figure 27.2: Illustration of the apparent over-representation of edge and line information. (top) Example from a sub-image of a fingerprint; notice how many local "line" responses are possible. (bottom) Cartoon abstraction of the situation at the top, in which many different cells within a column are responding, some to image structure and some to noise. Notation: Columns are drawn vertically above the image location defining receptive field center. The receptive fields are abstracted as lines in each column, each indicating the preferred orientation of the cell it represents. Thickness indicates response magnitude, e.g. spikes per second.

440 C. Blakemore and E.A. Tobin: Lateral Inhibition in the Cat's Visual Cortex

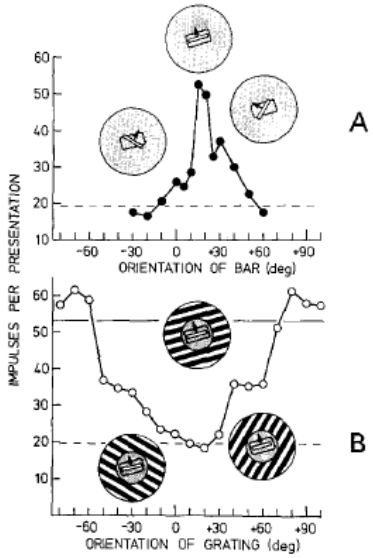

Fig. 1. The upper graph shows the orientational "tuning curve" in the left eye, for cell A6R1. The receptive field was 6.5 deg long and 2.5 deg wide and the arrangement of the stimulus is shown in the inset diagrams. The larger rectangle represents the receptive field and the smaller one is the moving bar. The luminance of the background was about 9 cd.m^{-2} and of the bright bar 30 cd.m^{-2}: its velocity was 5 deg. sec^{-1}. The ordinate shows the mean number of impulses (N = 8) produced during a gating period of 2.5 sec centred on the time for which the stimulus was crossing the receptive field. The dashed line shows the mean spontaneous activity of the cell (N = 8) during the same gating period, in the absence of a stimulus. For the lower graph the moving bar was always at the optimal orientation, 15 deg anticlockwise to the horizontal. The cell's response (mean of N = 8) is plotted as a function of the orientation of a background grating whose dark bars had a luminance of 3 cd.m^{-2} and bright bars 15 cd.m^{-2}. (So its average luminance was the same as that of the background for the upper graph.) The solid horizontal line shows the level of response (about 53 impulses per presentation) that the cell produced in the absence of the grating

Figure 27.3: Data from Blakemore's experiment.

27.2.3 Lateral Inhibition in Layer II-III

The Blakemore experiment shows lateral inhibitory networks running over a column. How might we build this up?

We start with Fig. 27.4. (a) Overall view of a number of orientation hypercolumns at positions i, j, k, etc. The activity can be thought of as a probability distribution along the column (shown as a graph up column i); we will start to think of this activity as the probability of label λ at i. (b) To appreciate this activity profile along the columns, we show an outline of the excitatory part of the classical receptive fields of neurons along the column and (c) the tuning curve for the one centered at horizontal. This holds only in the perfect case of isolated stimulus. (d) Receptive fields and (e) activity plot along column at position k. Because this column has neurons with rf's located just off the line stimulus (shown as the dot in (d)) the tuning curve is lower and shifted slightly. The question is how can this activity within and across columns be used?

The strong overlap among receptive-fields within a column suggests firstly that some type of interaction among them could remove (or reduce) some responses. In particular, the monotonic decline in response (as a function of orientation; Fig. **??**) for a cell whose receptive field is located right on an image stimulus suggests a WINNER-TAKE-ALL STRATEGY: if there is an optimal response at some orientation θ, and a weaker response at orientation $\theta - \epsilon$, and an even weaker response at orientation $\theta - 2\epsilon$, and so on, then letting the strongest response inhibit the others suggests that it could "win." Note that if all cells in a column were to mutually inhibit one another then that cell with the largest response would inhibit all the others to baseline levels; but they would not inhibit that strong cell completely to baseline. (There is an interesting question here regarding normalization of responses to keep them in a reasonable operating range.)

Lateral inhibitory network running over a cortical column. (What does this imply about neural connectivity? Should more excitatory or inhibitory synapses be expected? Etc.) One way to think about this is that, since the receptive fields involve filtering the image, and since the receptive fields cover an area, then in effect they are "blurring" out the data; the lateral inhibitory network "sharpens" the data. Thus we see that the same network ideas that were discussed earlier can be applied not only to image intensity values, as was done with *Limulus,* but to abstractions such as "probability that a neuron will fire" or "membrane potential."

The effect of this sharpening computation is to SUPPRESS LOCAL NON-MAXIMA over a neighborhood.

Cross-orientation inhibition discussion and references.

Computational Example

In general, of course, we are in a position to build a full network with support from an entire neighborhood not only a network with columns; this suggests the full relaxation abstraction; see Fig. .

To design such a network we need to know which neurons should be connected

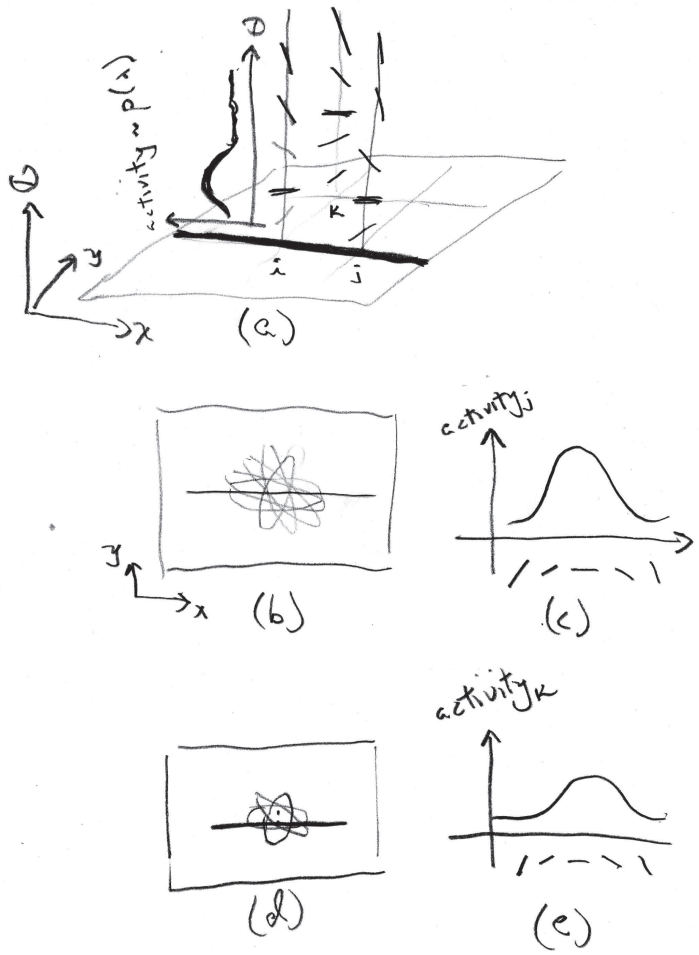

Figure 27.4: What does the response to a stimulus look like when projected onto the arrangement of neurons in columns. (a) Overall view of a number of orientation hypercolumns at positions i, j, k, etc. The activity can be thought of as a probability distribution along the column (shown as a graph up column i); we will start to think of this activity as the probability of label λ at i. (b) To appreciate this activity profile along the columns, we show an outline of the excitatory part of the classical receptive fields of neurons along the column and (c) the tuning curve for the one centered at horizontal. This holds only in the perfect case of isolated stimulus. (d) Receptive fields and (e) activity plot along column at position k. Because this column has neurons with rf's located just off the line stimulus (shown as the dot in (d)) the tuning curve is lower and shifted slightly. The question is how can this activity within and across columns be used?

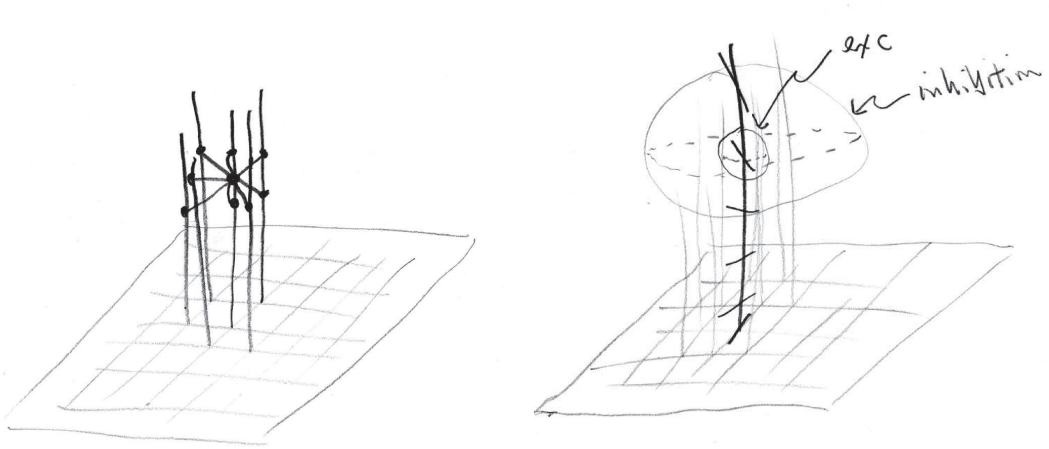

(a) (b)

Figure 27.5: Lateral inhibition across columns

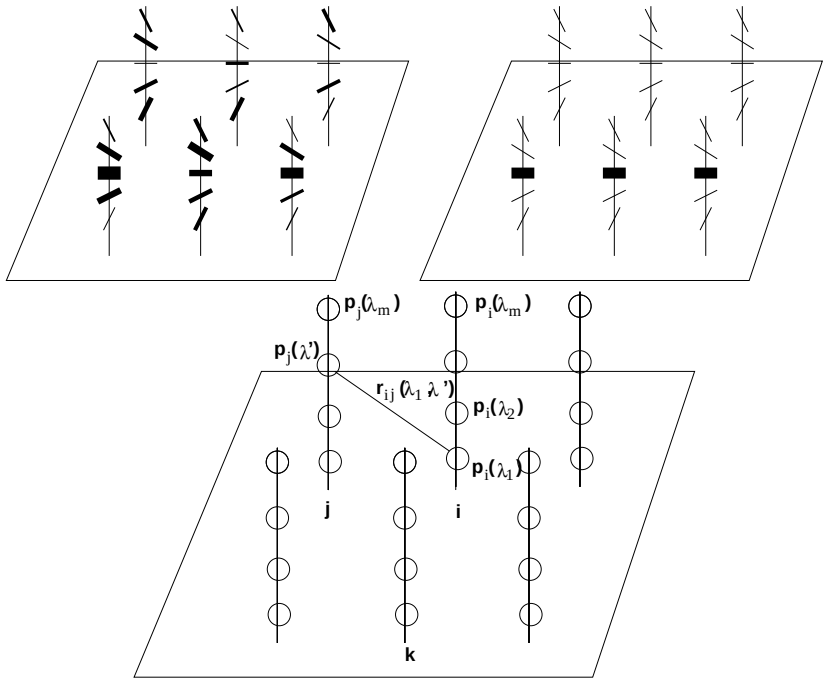

Figure 27.6: (top) Putative results of running a lateral inhibitory network along a column – the weak results are elimated and only the strong ones survive. But in general there is the question of how much

to one another and whether they are excitatory or inhibitory. How can the synaptic weights be set?

One way to answer these questions is to look in more detail to the neurobiology.

27.3 Long Range Horizontal Connections

We begin by taking a more detailed look at a superficial-layer pyramidal cell in V1; See Fig. fig:gilbert-lrhc(left). Its organization is suggestive of a regular connection structure with two important aspects.

1. *"short distance" connections*: many axonal-dendritic interactions appear clustered over short distances;

2. *"long distance" connections*: some axonal arborizations extend over longer distances.

The long-distance connections suggest that synapses are clustered around neurons in nearby columns; since they extend horizontally in cortex, i.e., since they remain in (approximately) the same layer, they are called LONG RANGE HORIZONTAL CONNECTIONS. If we could infer the structure of these connections then we could have some insight into which neurons were supporting one another for curve detection. In order to get this additional information we need to take a more detailed look at how orientationally selective neurons are arrayed in tangential directions. This becomes possible with optical imaging.

27.3.1 Optical Imaging

When neurons fire action potentials, they require metabolic activity to maintain energetic levels. This, in turn requires oxygen, so by imaging cortex with light tuned precisely to the wavelength absorbed by oxygenated hemoglobin it becomes possible to visualize those areas that are most active; Fig. 27.8. When visual cortex is exposed and imaged in this fashion, it becomes possible to make a "map" of appropriate activity.

Orientation-selectivity maps can be made in precisely this manner. In Fig. 27.9 we show how cortex is organized into a composite of ORIENTATION DOMAINS, consisting of numbers of cells tuned to about the same orientation.

The classical notion of column can now be understood as existing in a special sense in which an electrode penetration is made in certain directions (so that it passes though many different colors.)

Notice also that there are locations in which many colors/orientations seem to come together to form a PINWHEEL.

Similar maps have been made for spatial frequency selectivity (get image from Styker).

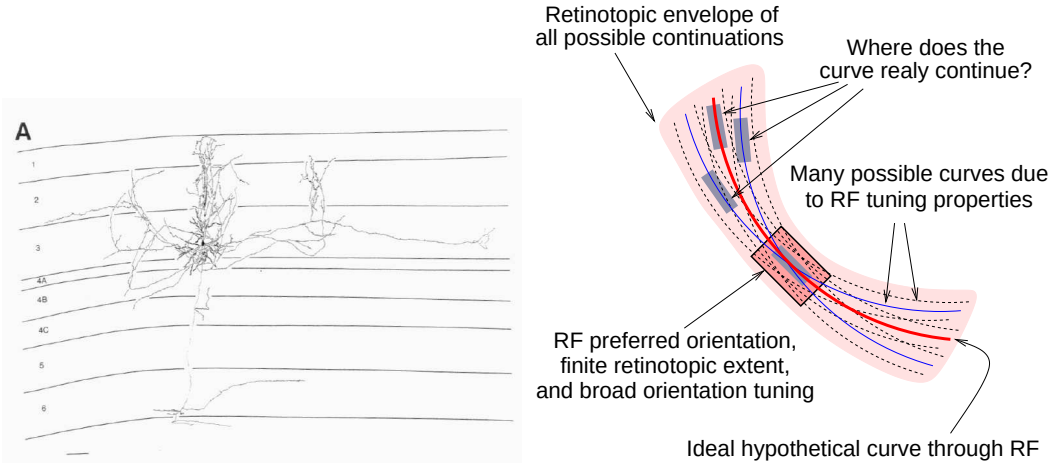

Figure 27.7: (left) Filled pyramidal cells from superficial layer V1 (C. Gilbert). Although the cell body is barely noticable, the well articulated axonal arborization is spectactular. It exhibits a telling organizational structure that suggests inter-columnar interactions. (right) Cartoon of implied receptive field locations for the target neuron shown (left) and a number of putative neurons to which it might connect.

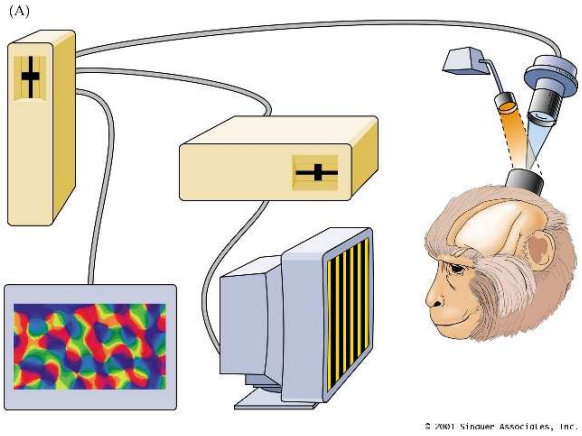

Figure 27.8: The set-up for optical imaging of visual cortex.

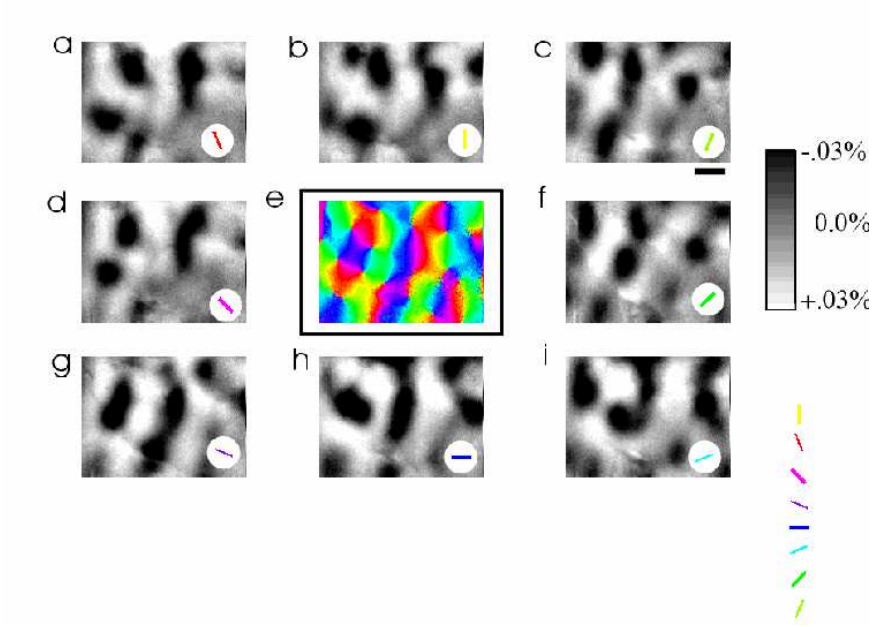

Figure 27.9: Illustration of the technique of optical imaging. This series of panels displays an image of cat V1 cortex with the camera focussed on the superficial layers while drifting sinusoidal gratings at different orientations are displayed. (The angle is shown as a colored bar inset.) From these individual masks a composite in color is made: color scale indicates orientation (see lower right.)

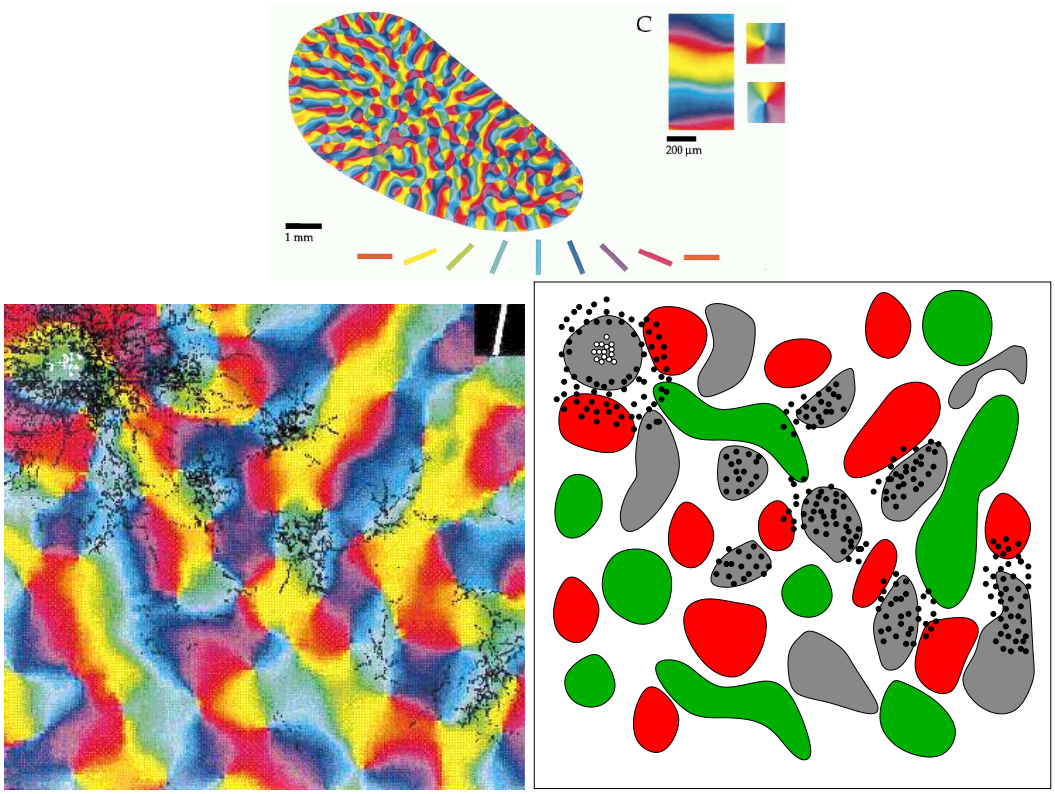

Figure 27.10: Fitzpatrick lab data from ferret. (top) Optical image map of cortex for orientation preference. (bottom) Composite image made with synaptic boutons superimposed onto the optical image. The technique is illustrated in the cartoon.

The anatomical tracing data can be placed together with the optical imaging data in a technique developed in David Fitzpatrick's lab; see Fig. 27.10.

At first glance this experiment suggests that a cell with a given orientation preference is likely to form synapses with other cells with similar–or identical–orientation preferences. To transform this observation into a quantitative form, the number of connections (represented by the count of the deposited boutons) can be plotted against the difference in preferred orientation between the "filled cell" and the "target cell;" See fig. 27.11. A striking interpretation emerges from the mean data, which reconnects modern neurophysiology to classical notions in Gestalt Psychology.

27.4 Does Gestalt Continuation Imply Co-linear Continuation?

Gestalt psychology in the first half of the last century studied visual perception as an example of how "the whole is more than the sum of its parts." This phrase has several

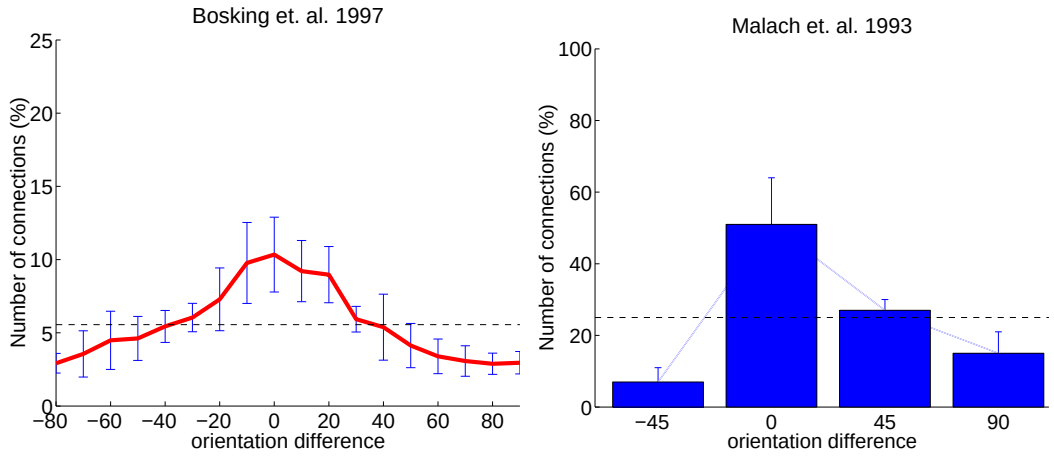

Figure 27.11: Fitzpatrick lab data (left) from ferret and Malach lab data (right) from primate. The red curve indicates the mean distribution across many experiments; as do the heights of the bar graph. Notice in particular that both distributions are peaked at 0 degrees offset; this first-order property of the data has dominated thinking about it.

important implications for our work, one of which is that a curve is somehow more than the pieces of which it is comprised. This is famously illustrated in the Gestalt concept of GOOD CONTINUATION; i.e., that the direction for continuing a curve is most likely to be the one in which the curve was last going. This is illustrated in Fig. 27.12 and would seem connected to the physiology just described. We first explore this connection is a basic way, then revisit the data with a more careful eye.

In a simple sense one could interpret the Gestalt observations in light of the Fitzpatrick physiology: the visual system is "wired up" to enforce good continuation for co-linear (or almost co-linear) segments.

Modern visual psychophysics would seem to confirm this. When small image patches that are designed to stimulate receptive fields are aligned to form "smooth" curves; i.e., curves in which the local patterns are roughly co-aligned, then such curves seem to POP OUT from a background of noise elements; see Fig. 27.13.

27.4.1 Experiments with Co-Aligned Facilitation

The natural interpretation of the Gestalt effects is to assume that the visual system is "wired" to prefer straight co-linear continuation, and to prefer a small angle to continuation a little less; a larger angle a little less, and so on. The fit for the Fitzpatrick mean data suggests a system of compatibilities as a Gaussian or perhaps an exponential model.

We built such a relaxation labeling system in 1977; results are in Fig. **??**. It was defined as follows:

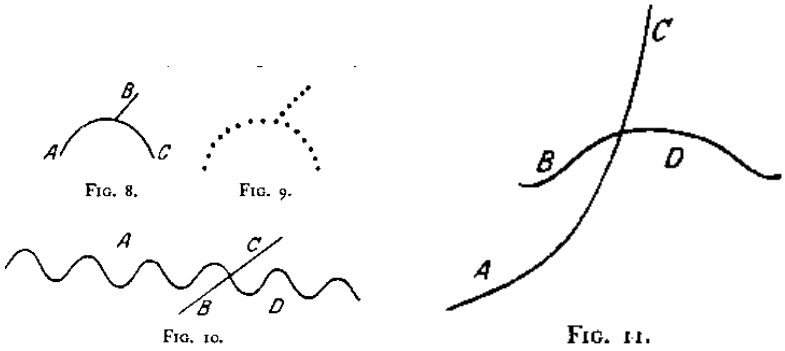

Figure 27.12: Imagine wandering along a curve such as those on the left side, even when it is a dotted curve. One tends to continue in the same direction. Problems can arise in choosing direction at crossings, because then there is a question of which branch to follow. Locally this can be quite confusing (right). Original drawings from Wertheimer 1923.

- Objects $(i, j, k, ...)$: image pixel locations;
- Labels: $(\lambda_1, \lambda_2, ..., \lambda_8)$: line orientatations;
- Neighborhood relationship: Gaussian over nearest neighbors?
- Compabitilities: Roughly, a skewed distribution over orientation differences; see table 1 below.

Results are in Fig. 27.14

Table 1: Gestalt compatibilities for line enhancement

angle diff between λ and λ'	0	22.5	45	67.5	90
$r_{ij}(\lambda, \lambda')$	1.0	0.5	0.05	-0.15	-0.25

Another series of experiments can be obtained from the computer-vision standard edge detector system developed by Canny; this prefers to continue along the preferred direction according to an "optimal" formula that depends on strength of operator response and an inertia term. Only the single, most approapriate edge value is retained at each position. Typical results in Fig. 27.15. Given the manner in which this destroys the basic surface topology it would seem that something more must be done.

27.5 Why Columns? A first look

Although there is a question of how the compatibilities were defined in Table 1, and their performance on a curve detection task, we now ask about the "good news"

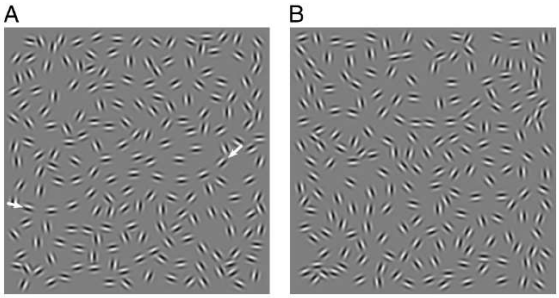

Fig. I. Embedded contours. (A) a contour path (marked by white arrows) is embedded in similar background elements (see text for details). **(B)** Only the background elements are shown, but the local density is the same as in A.

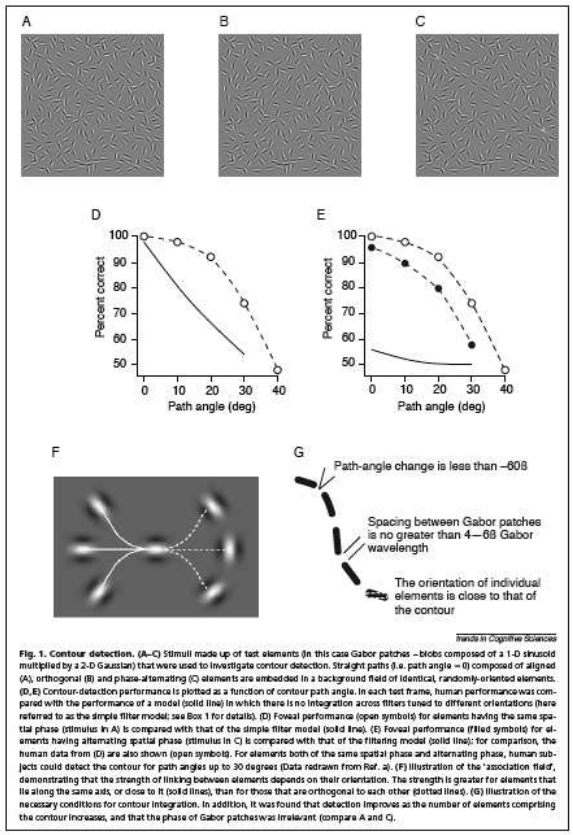

Fig. 1. Contour detection. (A–C) Stimuli made up of test elements (in this case Gabor patches – blobs composed of a 1-D sinusoid multiplied by a 2-D Gaussian) that were used to investigate contour detection. Straight paths (i.e. path angle = 0) composed of aligned (A), orthogonal (B) and phase-alternating (C) elements are embedded in a background field of identical, randomly-oriented elements. (D,E) Contour-detection performance is plotted as a function of contour path angle. In each test frame, human performance was compared with the performance of a model (solid line) in which there is no integration across filters tuned to different orientations (here referred to as the simple filter model; see Box 1 for details). (D) Foveal performance (open symbols) for elements having the same spatial phase (stimulus in A) is compared with that of the simple filter model (solid line). (E) Foveal performance (filled symbols) for elements having alternating spatial phase (stimulus in C) is compared with that of the filtering model (solid line); for comparison, the human data from (D) are also shown (open symbols). For elements both of the same spatial phase and alternating phase, human subjects could detect the contour for path angles up to 30 degrees (Data redrawn from Ref. a). (F) Illustration of the 'association field', demonstrating that the strength of linking between elements depends on their orientation. The strength is greater for elements that lie along the same axis, or close to it (solid lines), than for those that are orthogonal to each other (dotted lines). (G) Illustration of the necessary conditions for contour integration. In addition, it was found that detection improves as the number of elements comprising the contour increases, and that the phase of Gabor patches was irrelevant (compare A and C).

Figure 27.13: Field Hayes Hess experiment.

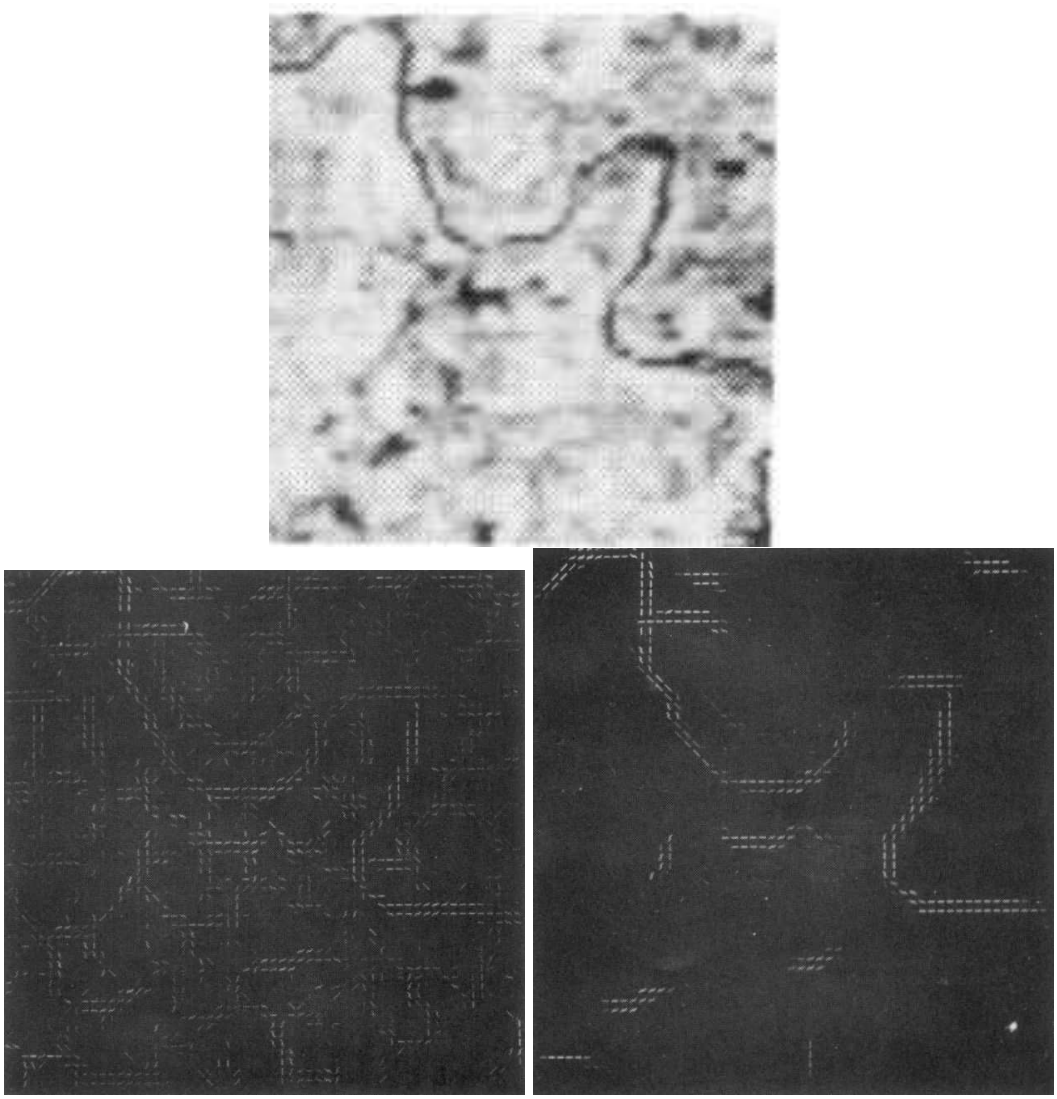

Figure 27.14: Results of applying a relaxation labeling system that prefers "straight" continuations to a LANDSAT image of a river. (left) initial line-detector responses. (right) converged result (5 iterations). Note that while the river is recovered, a subtle geometric distortion has occurred: places of high curvature have been "broken" into discontinuities. Recall how this type of result reminds us of the scalloped views in stereo algorithms that prefer the frontal-parallel plane solution.

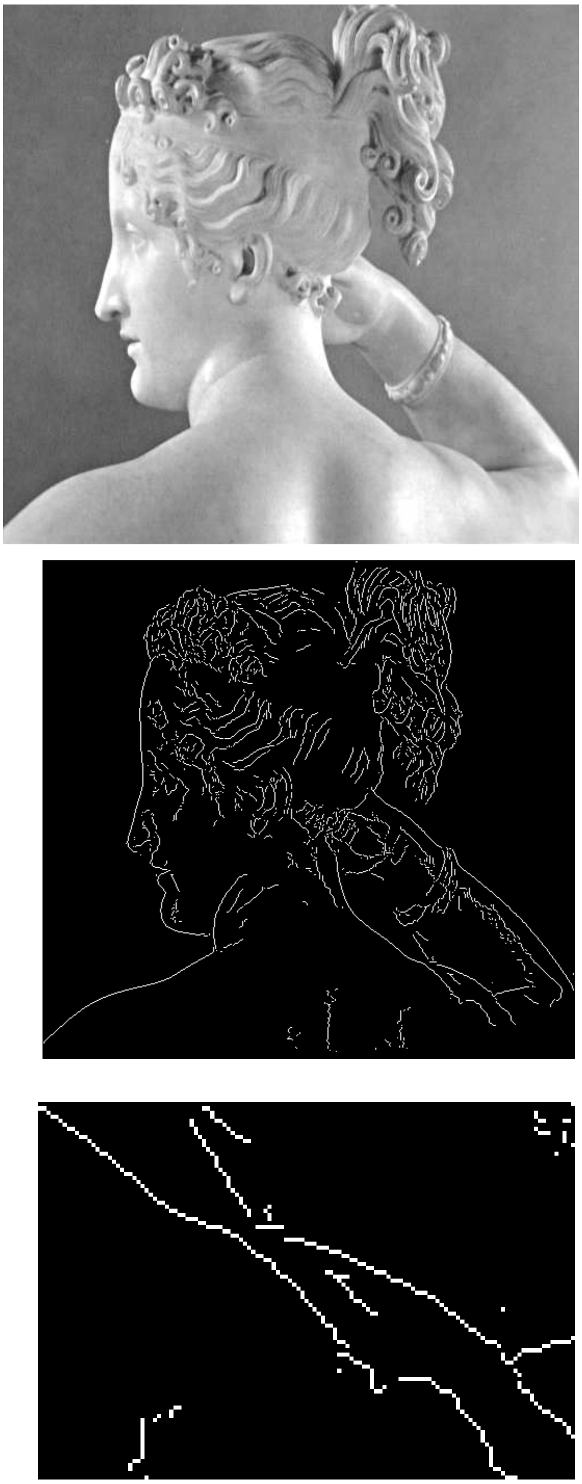

Figure 27.15: Results of applying the Canny edge detector to an image of the Canova sculpture. (top) Original image. (Middle) Canny edges. (bottom) Blowup of the area around her right shoulder – can you determine the proper connectivity relationships to define the shoulder?

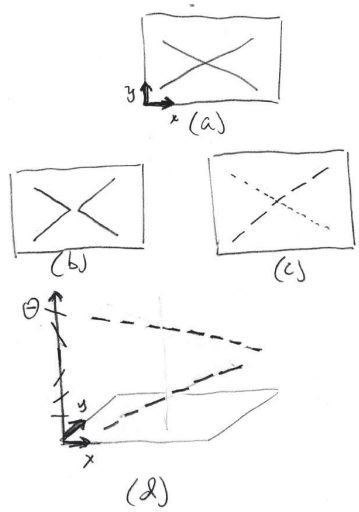

Figure 27.16: A advantage of columnar representations is that non-simple points of curves, such as the crossing point between the two lines in (a) are separated. Earlier we raised the question of whether this was a non-generic view of (b); i.e., two separate crossing lines as shown in (c). When *lifted* into (x, y, θ)-space, notice how the two lines naturally separate in level (because they are at two different θ heights. This suggest that we think of orientation good continuation not in (x, y) space alone, but in the elaborated (x, y, θ)-space.

regarding columns: why is cortex organized in this columnar fashion? Issues that have already come up include (i) over-redundant representations and (ii) the emergence of a cortical computational machine. Both will turn out to be important in future lectures.

We highlight one emergent property of columnar representations, and it goes back to the Gestalt examples presented earlier. Consider the example in Fig. 27.16 of two crossing lines. A key issue before was why this appeared as the "generic" crossing lines rather than the "non-generic" or highly specialized pair of "V's" exactly arranged. Now we see that representing this crossing pattern in (x, y, θ) elaborates the "X" into two separate lines (separated because they are at different angles, i.e., at different heights.) Good continuation is thus naturally developed in the (x, y, θ)-space. We shall have much more to say about this space in subsequent lectures.

27.6 Non-Monotonic Variance in Connection Data

We end this Chapter with a deeper view of the statistics on connections from the Fitzpatrick laboratory. Notice that while the mean value curve was easily explainable,

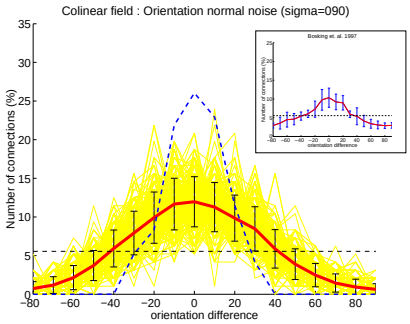

Figure 27.17: Monotonic variance across connections is to be expected from noise in a learning process that seeks to connect co-aligned cells.

the variance across experiments is not. In particular, the variance across experiments, which amounts to a variance across cells (since different cells are filled in each experiment) is strongly non-monotonic: it peaks at 0 offset in orientation; it is minimal around $\pm$ 30 degrees, and then it gets larger again.

To what might this non-monotonicity in variance be attributed? One possibility is that the visual system, when it "learns" the wiring is seeking to connect co-aligned cells but deviates from this because of inefficencies or noise or some other random variation. This cannot be the case, however, because such schemes produce a monotonic decrease in variance; see Fig. 27.17.

Maybe there's something deeper to this non-monotonic variance and maybe it's connected to how the connections should be learned – or defined. We turn to these questions in the next few lectures.

27.7 Summary

We shall have to take a deeper look to understand the biology (non-monotonic variance) and to develop systems that properly detect boundaries.

Part VII

Section VII: Curvature as a Constraint

We now have a language set up for neural computation – columns and long-range connections – so now we need to be clear about what are the units and how they combine.

Key role for the mathematical notion of curvature, leads us to revisit many of the earlier problems.

Chapter 28

Curvature, Co-Circularity and the Geometry of Connections

Connections in columns, (position, orientation) space; orientation selectivity and tangents; endstopping and curvature; co-circularity; non-monotonic variance revisited;

28.1 Introduction

In this lecture we relate the mathematical properties of curves, basically their differential geometry, with our developing model of visual cortex.

When dealing with curves and surfaces previously, we used various notions informally: orientation, and even the word curve itself. To make progress we shall now consider more deeply what these words mean. This will involve revisiting derivatives and tangents, and how they are related.

Establishing the connection between these mathematical ideas and the long-range connections from neurobiology is our goal. We shall move well beyond the "co-aligned facilitation" considered two lectures ago.

To set the stage, we relate the previous cartoons in which long-range horizontal connections related cells in the orientation domains defined optically with the original Hubel-Wiesel cartoon of orientation columns. In Fig. 28.1 we show the Fitzpatrick lab view in the lower panels and the tangential penetration view in the upper panels.

Two fundamental observations arise.

- When we consider the "column" of cells comprising an orientation column as lying over the retinotopic location at which the receptive fields are centered, then a new coordinate system emerges. There are the (x, y) coordinates of the retinotopic (or image) plane but there is also a θ coordinate against which the orientation preference of the cell is plotted. Thus a fuller model is to consider the coordinate system (x, y, θ) which takes values in $\Re \times \Re \times S^1$, where S^1 is the unit circle.

· Working within (x, y, θ) coordinates the long-range connections take on a more direct meaning: we must now directly confront the fact that they relate an orientation at one position to a (possibly different) orientation at a different position.

In effect, one might start to develop an intuition that these connections indicate how the orientation is changing as we move along the curve, and how this might help to disambiguate some of the confusion illustrated previous; see Fig. 28.2. If we move a tiny step; i.e., if all the distances are small, then a type of differential analysis can be applied. This is how we begin, by determing how to apply differential analysis to a curve. Our starting point builds on the previous lecture: that is, to apply the geometric interpretation, we identify the output of orientation-selective cells in V1 with tangents to curves. As we now show, this identification has non-trivial consequences.

28.2 What is a Curve?

We now undertake a more systematic treatement of curves. Consider a point moving through an image; in the spirit of Newton a curve can be thought of as the positions $\alpha(t) = (\alpha_1(t), \alpha_2(t))$ in Euclidean 2-space swept out by a moving point α at parameter (time) t. Provided the coordinate functions $(\alpha_1, \alpha_2, \alpha_3)$ are differentiable, a *curve* can be defined as a differentiable map $\alpha : I \to \mathbb{E}^2$, from the open interval I into $\mathbb{E}^2$. For now we shall assume the curve is simple, i.e., it does not cross itself, so the map is one-to-one and is an *immersion* of I into $\mathbb{E}^2$. See Fig. 28.3.

The derivative of the map α gives the velocity or *tangent vector* of α at t (Fig. 28.3):

$$\alpha^{'}(t) = (\frac{d\alpha_1}{dt}(t), \frac{d\alpha_2}{dt}(t), \frac{d\alpha_3}{dt}(t),)_{\alpha(t)}$$

A curve is *smooth* provided these derivates exist and is *regular* provided these derivatives are not zero simultaneously.

Since the derivative is the best linear approximation to the curve; identifying it in the proper way with the output of an orientation-selective neuron is natural.

A reparameterization $s = s(t)$ yields the arc-length (unit speed) parameterization in which the length of each tangent vector is 1. We denote this unit speed curve by $\beta : I \to \mathbb{E}^3$ with $||\beta^{'}(s)|| = 1, s \in I$.

We are interested in direction and, for non-straight lines, the rate at which the curve is bending. Intuition is helped by picturing the unit tangents as vectors in $\mathbb{E}^3$ attached to the points $\beta(s) \in \mathbb{E}^3$, that is, as a vector field along the curve. Euclidean coordinates for this vector field can again be differentiated:

$$\alpha^{''}(t) = (\frac{d^2\alpha_1}{dt^2}(t), \frac{d^2\alpha_2}{dt^2}(t), \frac{d^2\alpha_3}{dt^2}(t),)_{\alpha(t)}$$

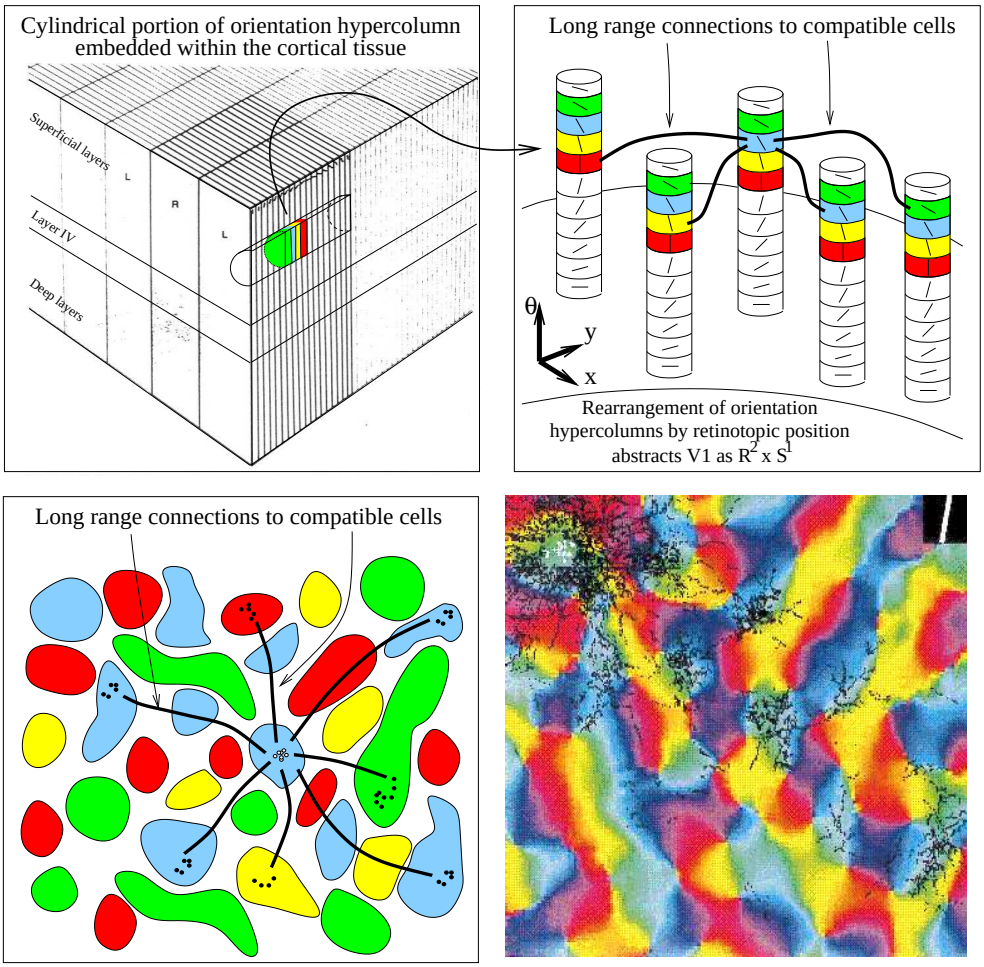

Figure 28.1: Relating the tangential penetration view of orientation columns with the long-range horizontal connections leads to the conclusion that, in the simplest terms, they encode relationships between an cell preferring one orientation at a retinotopic location with another (possibly different) orientation at a nearby location. Our goal in this chapter is to exploit this relationship by developing the consequences of working in (x, y, θ)-space. It is important to remember that, while the co-linear facilitation model could explain the peak of connections between cells preferring the same orientation, it could not explain the *variance* across different cells. There must be more to the story—even for curves.

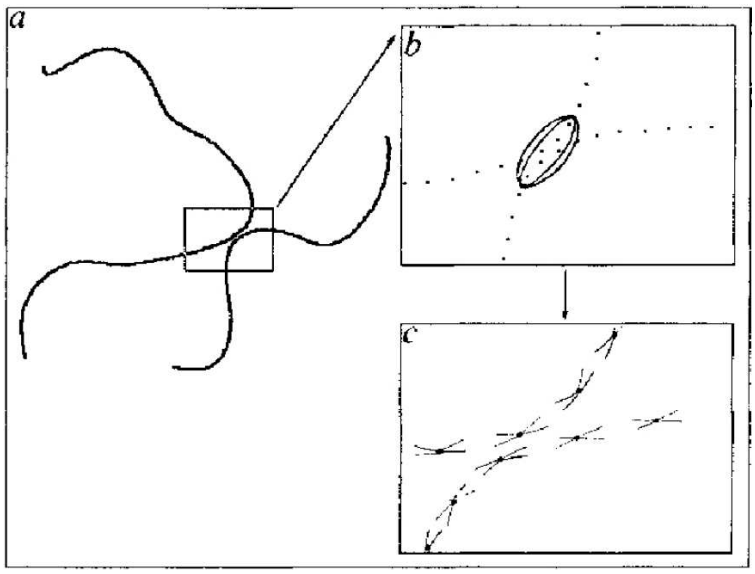

Figure 28.2: Information about how a curve is curving can help to restrict its extension, thereby providing some constraint for curve inference. In this lecture we seek to develop this intuition about curvature: what it is; how it can be used; and how it might be represented neurobiologically.

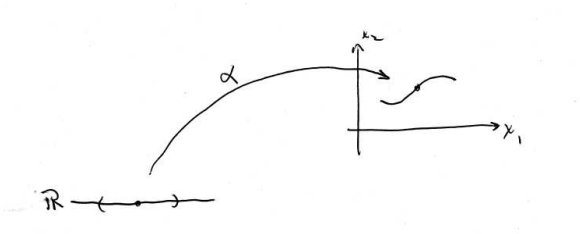

Figure 28.3: (left)Definition of a curve as a map from a parameter space, I, to the plane. I is shown as a set, which is part of the real line. Each point in this plane can be specified by a vector from the origin so that it is Euclidean. The parameter $t \in I$ denotes position along the curve; the derivative at a point is the tangent vector. For an arc-length parameterization we take the interval to be closed, and define a parameter that starts at a = 0 and ends at b = 1.

to yield the acceleration, the rate of change of velocity. In geometric terms, since the velocity corresponds to the tangent, the rate of change of the tangent corresponds to the curvature.

28.2.1 The Osculating Circle

A more intuitive picture of curvature can be obtained by revisiting the classical limiting operation from calculus; see Fig. 28.4. In this case we consider two nearby points, p_1 and p_2, with tangents T_1 and T_2, respectively. Orthogonal to these tangents are the normals, N_1 and N_2, which intersect at the point M. For the limiting operation, let p_2 approach p_1 along the curve. The angle between the tangents is the same as the angle between the normals, and it approaches a limit:

$$\lim_{P_1P_2 \to 0} \frac{\angle(N_1, N_2)}{P_1P_2} = \kappa$$

Moreover, M is a distance $r = 1/\kappa$ from the limiting point.

Thus, curvature is a relationship between tangents at nearby positions; it indicates how the tangent angle rotates as the point of attachment is moved along the curve.

28.3 Coordinate Free Definition of a Tangent

Although the mapping view is important for analysis, it leaves open a question of how to relate it directly to receptive-field structure. Observe that, no matter which curve was passing through a receptive field center, the only point that matters is that it remain within the center. Thus there is an equivalence class of curves that would all cause the neuron to fire; and this equivalence class structure can be used to develop a "coordinate free" definition of the tangent.

To start the process, look at the tangent to a sector of a circle in Fig. 28.5(left). Here it looks like the tangent can be described as a line orthogonal to the vector from the center of the circle. But notice, importantly, that this tangent line rapidly leaves the circle. In effect it lives in the (x,y) plane in which we drew the circle (as does the circle).

The coordinate-free notion of a tangent is the equivalence class of curves passing through a point such that their derivatives (expressed in any appropriate chart) are equivalent. And this holds for curves drawn on surfaces or other higher-dimensional manifolds. Thus we have succeeded in defining a notion of tangent (which does not necessarily line on a curve) in terms of curves!

28.4 Co-Circularity and Connection Fields

We are now in a position to apply these geometric ideas to the curve inference problem. Suppose the different orientation responses correspond to possible tangents along a

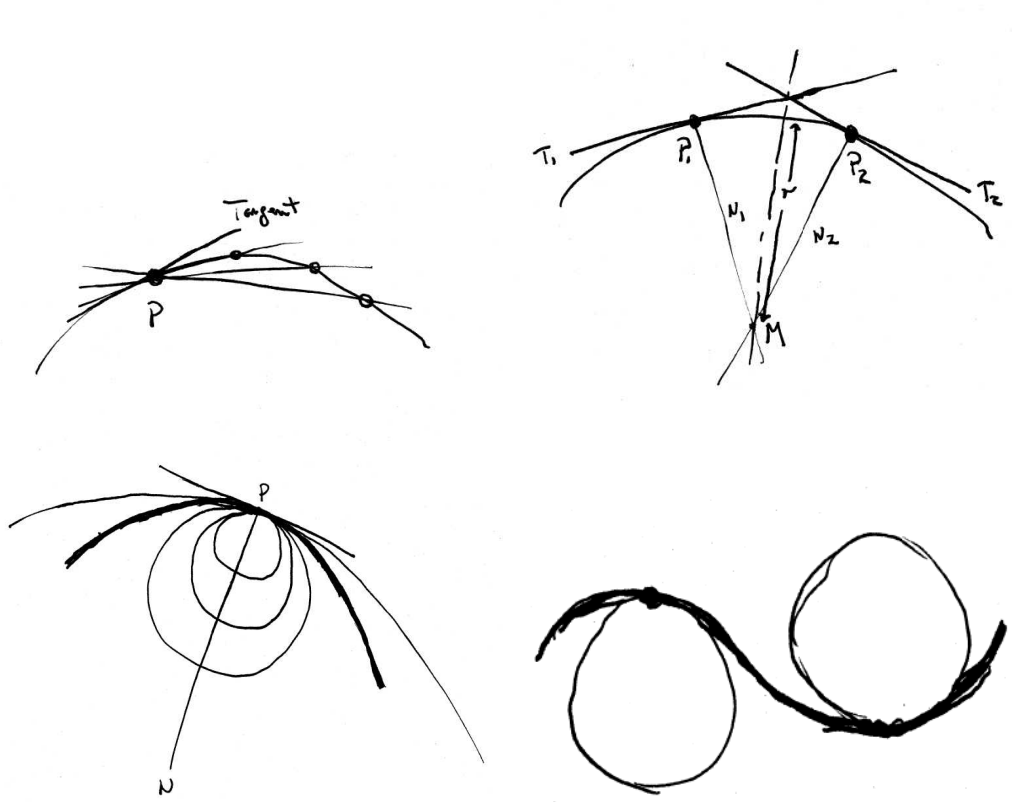

Figure 28.4: (top, left) Classical notion of the tangent as a limiting secant, taking the limit from the right. (top, right) If this process is repeated at another point, then two tangents are obtained. The angle between them, normalized by arc length, is the curvature. (bottom, right) A higher-order contact structure is obtained by fitting a circle to the curve at a point, such that the tangent to the circle and the tangent to the curve coincide. This *osculating circle* enjoys at least 3 point contact with the curve. (bottom right) If we traverse the curve in a particular direction, the side on which the osculating circle lies is determined by the sign of curvature. Constructions after Hilbert and Cohn-Vossen.

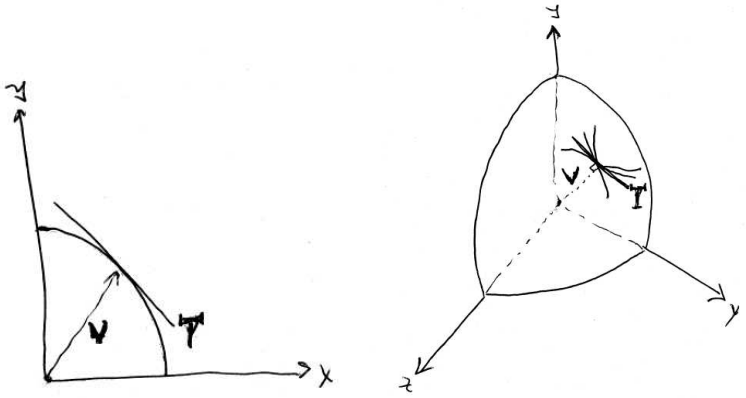

Figure 28.5: (left) The tangent to a circle is orthogonal to a radius vector, but extends off of the circle. (right) In general curves on a sphere (or, more generally a surface) can be used to define a tangent via equivalence class structure.

curve; our task now is to determine which of these possible tangents agree with the curve data. Since we seek to infer the actual curve, or a representation of it, we can't simply check the measured tangents against it. However, we can relate nearby tangents to one another. If the curve were known, then this would be an elementary operation: simply take the tangent at one position and move it along the curve to a nearby position while rotating it appropriate; if it agrees with the tangent measured at this new position then the two agree with the curve; we shall say the two tangents are consistent with one another. If it does not agree, then the two tangents are inconsistent with one another.

The flaw in this reasoning, of course, is that the curve is unknown. But we can exploit the above geometry to work not with the curve itself, but rather with an approximation to it given by the osculating circle. The movement can then be along the osculating circle instead of the curve, provided we can get an estimate of the osculating circle. This relationship is called CO-CIRCULARITY; see Fig. 28.10. The substrate for representing curvature is the endstopped property of orientation-selective cells, which we discuss in the next Section.

Precomputing these transports gives us the compatibility fields for an individual neuron. See Fig. 28.7.

With these compatibility fields, we can construct a full relaxation labeling system; results in Fig. **??**.

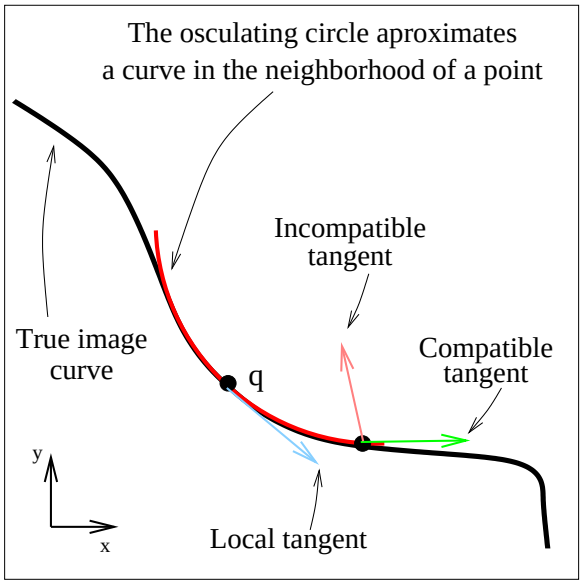

Figure 28.6: The geometry of co-circularity and the compatibility of tangents.

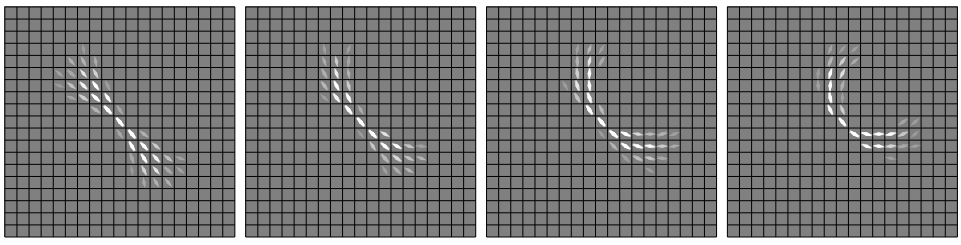

Figure 28.7: Co-circular compatibility fields. Only the excitatory components are shown. These are mathematical approximations of the transport of tangents for a short distance along a curve. Equivalently, these are mathematical approximations of the long-range horizontal connections between cells with different orientations.

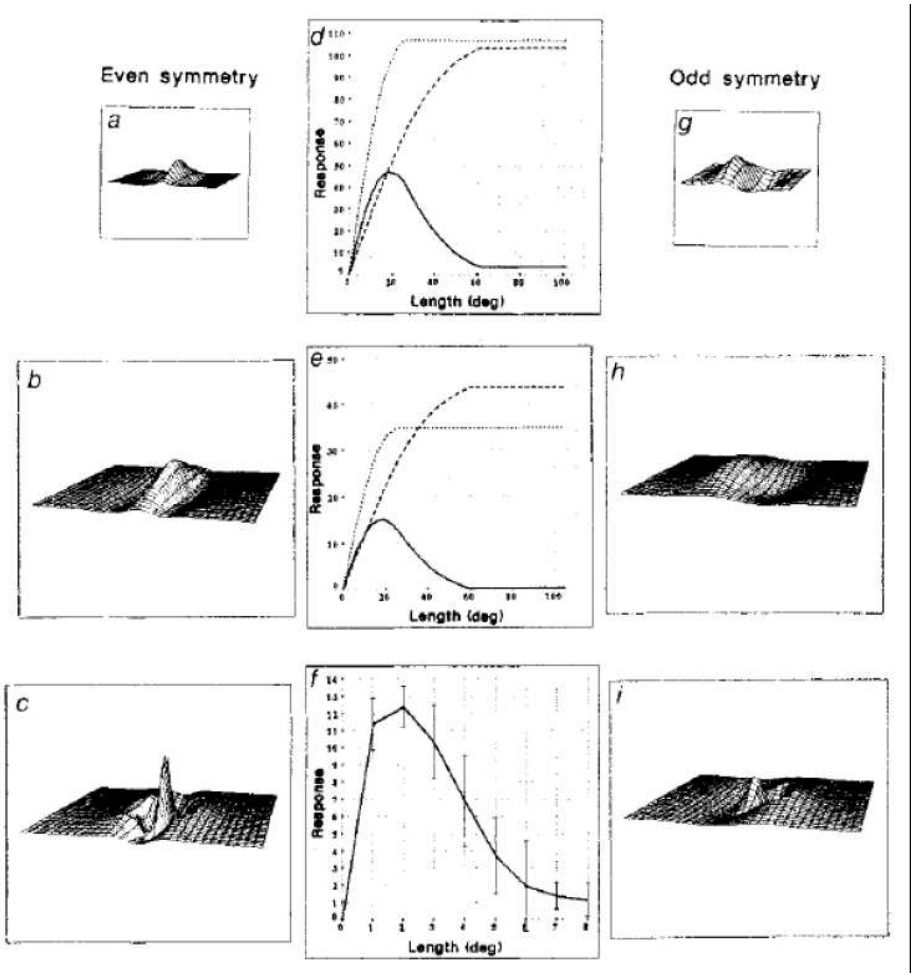

Figure 28.8: Cartoon form of the Dobbins model for estimating endstopping. Explain

28.5 Endstopping and Curvature

We earlier catalogued the different properties to which visual cortical neurons were selective. While we concentrated on orientation selectivity quite a bit, we now turn to a much less-well studied (and often ignored) property, endstopping.

Recall that endstopping is the property of response reduction with increasing length of the stimulus. One can think of this reduction as deriving from inhibitory "endzones" on either end of the classical receptive field. In the simplest schematic sense these endzones could derive from a circuit in which a large receptive field at the same location as a smaller one, and tuned to about the same orientation, were combined in an inhibitory manner; see Fig. 28.8

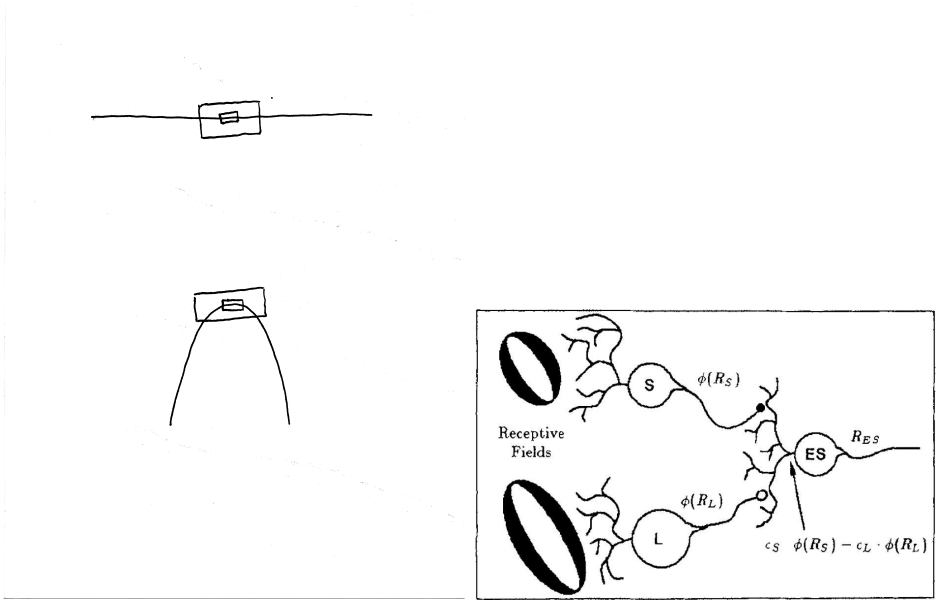

Figure 28.9: Cartoon form of the Dobbins model for estimating curvature. (left) In the top figure we show a straight line stimulus and bottom a curved stimulus. Notice how the small cell responds well to both stimuli, but the large cell only responds well to the top stimulus. In the lower case the stimulus enters the inhibitory sidezones which reduce response. (Subzones in rf's not shown.) (right) A simple circuit realization of eq. XXX in text.

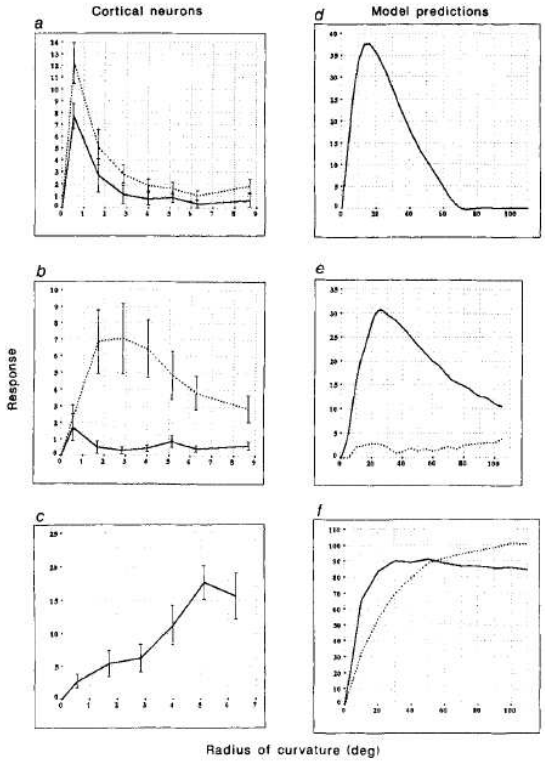

Figure 28.10: Data from Dobbins, 87, indicating a bandpass response to arcs of circles; i.e., to curvature.

28.6 The Co-Circularity Relaxation Labeling System

description of system here.

28.6.1 Experimental Results

With these compatibility fields, we can construct a full relaxation labeling system; results in Fig. 28.11.

28.6.2 The Co-Circularity Manifold

Viewing co-circularity functionally as a relationshop between positions, orientations, and curvatures; in effect the 6 degrees of freedom are constrained to live on an embedded submanifold with only 3 degrees of freedom.

28.6.3 Gestalt Good Continuation in Columns

To propertly understand Gestalt good continuation even for orientation, it is necessary to have a richer view of how it relates to cortical architecture.

28.7 Co-Circularity Predicts Long-Range Horizontal Connections

Given that we have a model for long-range connections, we can now envision this in the hypercolumn representation; see Fig. 28.13. As such, it is formally analagous to the connection structure we had previously sketched.

An important computation we can do with this model is precisely the experiments carried out in the Fitzpatrick laboratory; remarkably, we obtain precisely the same statistics! See Fig. 28.14. This holds as well for individual cells and argues strongly against the association-field model obtained from psychophysics (there is no variance from that model).

We can see the relationship between co-circularity and association fields, however. Since the psychophysics "averages" over tasks, in effect the association field is the average of the "union" of the co-circularity fields.

28.8 The Frenet Equations

The full structure of the co-circularity construction is most elegantly formulated in modern differential-geometric terms. The key idea is to express the intrinsic structure of the curve in terms of an attached (tangent, normal)-frame; see Fig. 28.15

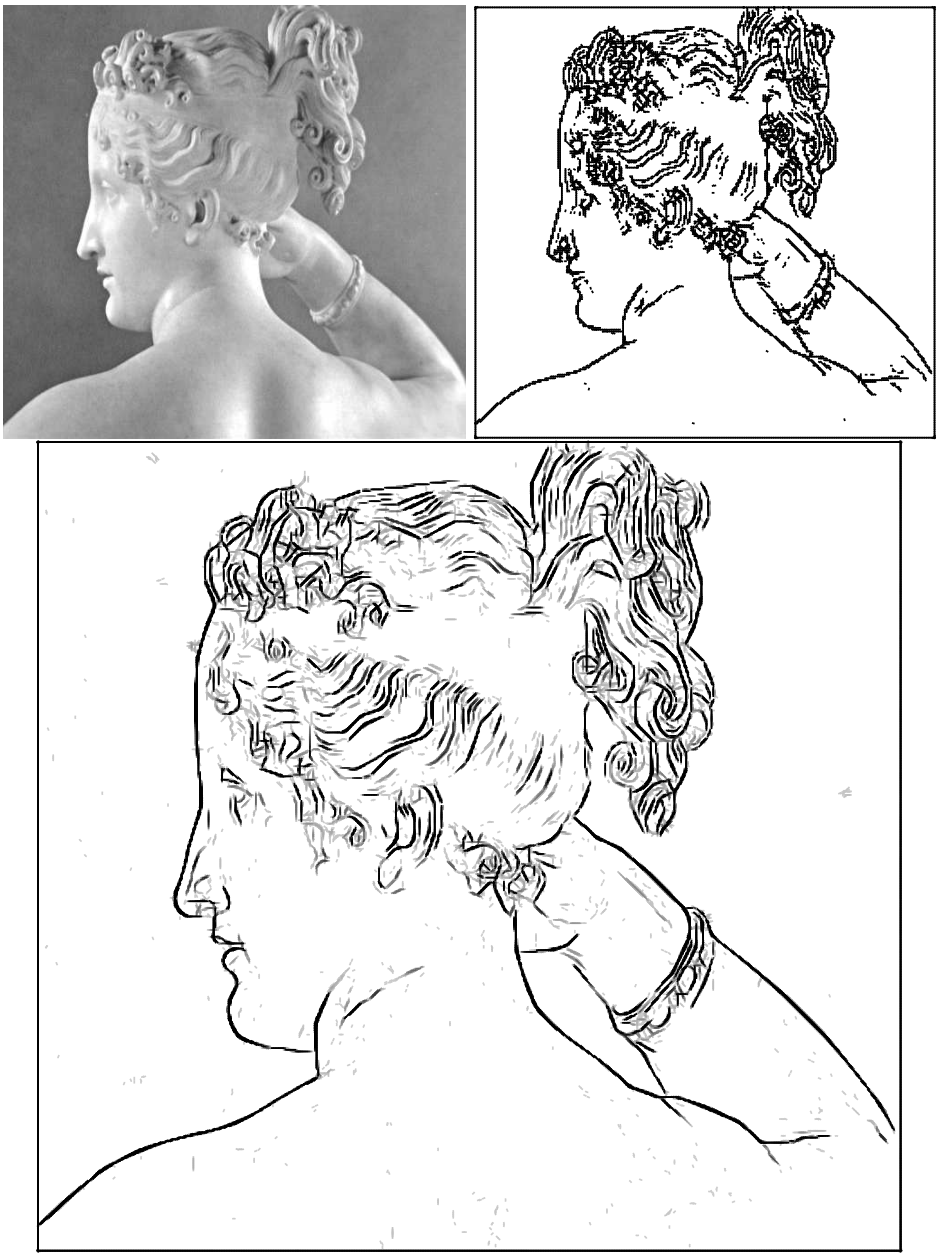

Figure 28.11: Example of running the relaxation labeling system on the upper image of Paolina. Notice in particular how the surface geometry, e.g., around the right shoulder musculature, is now clearly represented in much the way that an artist might do it. To achieve this class of results we not only needed a characterization of inter-columnar interactions, but we also needed a better set of initial responses (shown upper right). The non-linear technique for doing this is developed in the next chapter. (Compare against the Canny results in Fig.XXX.)

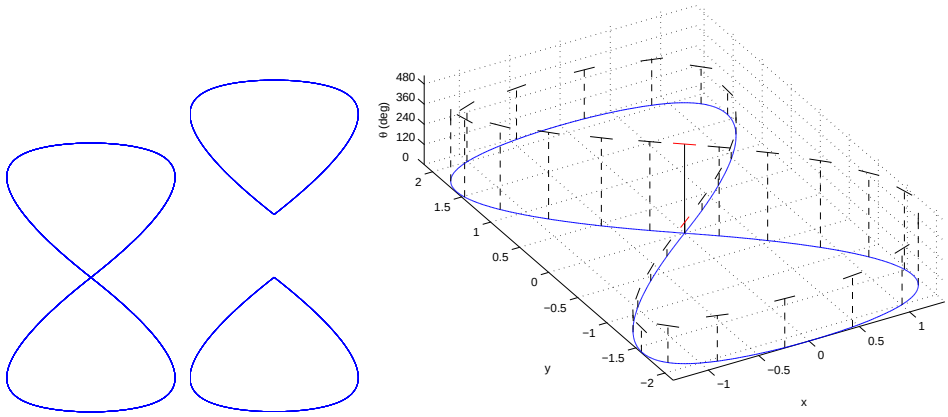

Figure 28.12: (left) The *figure-8* is a classical non-simple curve, which is rarely seen (middle) as two irregular curves meeting precisely at a point. (right) When lifted into a columnar-like representation it takes on a very different form that is now simple in the technical sense that it no longer crosses itself. Conclusion: one advantage of the lift into (position, orientation) space is representation of non-simple points along curves.

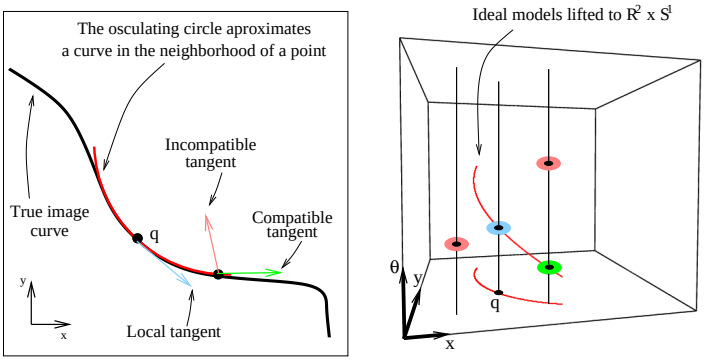

Figure 28.13: (left) The co-circularity construction in the image plane. (middle)The co-circularity construction lifted into the (x, y, θ)-representation (right).

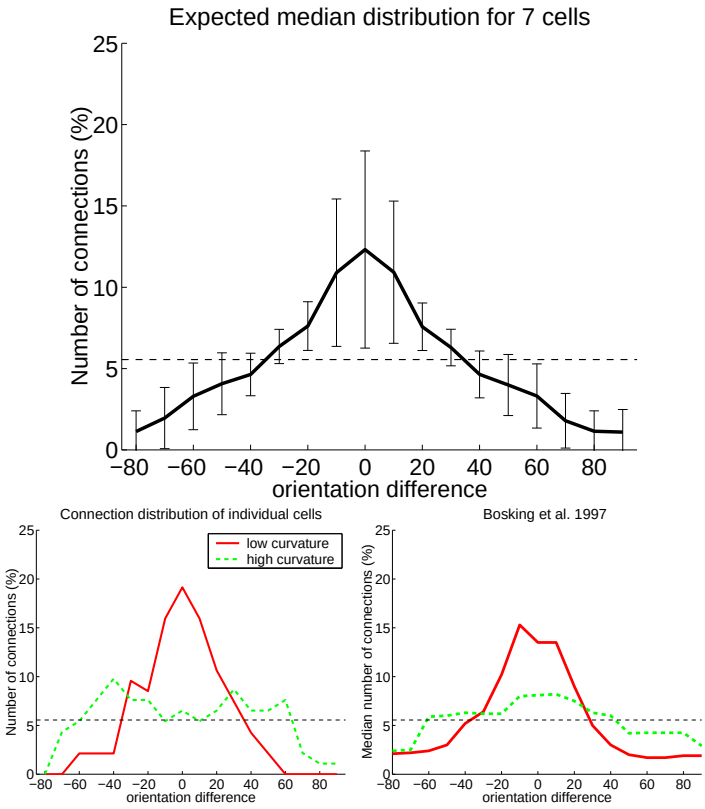

Figure 28.14: (top) Results of running the computational analog to the Bosking/Fitzpatrick experiment on the model for curve contination by co-circularity. Notive that the mean curve peaks at 0 offset; and that the variance in non-monotonic is the correct fashion. Thus the co-circularity model has predicted the neurobiological data through second order. (bottom left) Individual cells connections from the co-circularity model. (bottom right) Individual cells from the Fitzpatrick data. Note the similarity between the two examples chosen; the differences over these cells (either biological data or computational data) is what is responsible for the variance above; and is also a demonstration that the association field model cannot be correct.

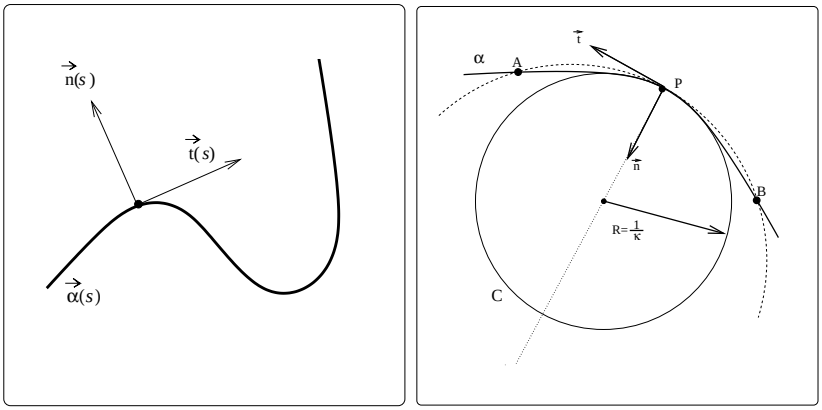

Figure 28.15: Two ways to think about the local structure of a curve in the plane. (left) The Frenet Frame is a (tangent, normal) coordinate frame that is adapted to the local structure of each point along a curve; and (right) the osculating circle is that circle with the largest contact with the curve among all circles tangent at that point.

Previosly we simply differentiated the curve (as a map) to yield the acceleration, but geometrically the following construction will be more useful. Let $\beta(s)$ be a unit-speed curve. Denoting the unit tangent $T = \beta'$ to obtain $T' = \beta''$, the curvature vector field. Observe T' is orthogonal to T by differentiating $T \cdot T = 1$. The direction of the curvature vector is normal to β, and its length $\kappa(s) = ||T'(s)||, s \in I$ is the *curvature*. The vector field $N = T'/\kappa$ defines the *principal normal*.

The *Frenet frame field* on β is the pair (T, N) such that $T \cdot T = N \cdot N = 1$, all other dot products $= 0$.

The remarkable property of this construction is that the derivatives of the frame can be expressed in terms of the frame itself. For curvature $\kappa > 0$ we have:

$$\begin{pmatrix} T' \\ N' \end{pmatrix} = \begin{bmatrix} 0 & \kappa \\ -\kappa & 0 \end{bmatrix} \begin{pmatrix} T \\ N \end{pmatrix}. \tag{28.1}$$

These are the famous Frenet-Serret formulas. It is in this sense that the Frenet frame is adapted to the individual curve in a way that captures its essential (differential) geometric structure.

Basically all of information about the curve is contained in the Frenet-Serret formulas. The following theorem is fundamental in differential geometry: Let $\kappa : I \to \mathbb{R}$ be continuous ($\kappa(s) > 0, s \in I$). Then there is a curve $\beta : I \to \mathbb{E}^2$ with curvature function $\kappa(s)$. Any two such curves differ only by a proper Euclidean motion.

Writing the Taylor approximation to the curve in the neighborhood of $\beta(0)$, and then substituting the Frenet formulas above and keeping only the dominant terms,

we obtain:

$$\beta(s) \approx \beta(0) + s\beta'(0) + \frac{s^2}{2}\beta''(0) + \frac{s^3}{6}s\beta'''(0) \quad (28.2)$$

$$\approx \beta(0) + sT_0 + \kappa_0\frac{s^2}{2}N_0 \quad (28.3)$$

Quality of approximation.

28.9 Co-Circularity in $\mathbb{R}^2 \times S^1$

We now focus on curves in the plane $\mathbb{E}^2$. Observe that the first two terms in the Frenet approximation give the line in which the tangent (or best linear approximation) lies; the first three terms give the best quadratic approximation (a parabola) which, expressed in the (x,y) plane, has the shape $y = \kappa_0 x^2/2$ near $\beta(0)$.

The quadratic approximation around a point is determined by the curvature at that point, which can be defined in another way. Suppose the curve is not straight, and choose any three points on β in the neighborhood of $\beta(0)$. Taking the limit as the three points approach $\beta(0)$, the *osculating circle* at that point is obtained. This is the unique circle tangent to the curve at that point such that its center lies on the normal and its radius is the inverse of the curvature (Fig.**??**).

The quadratic parabola is approximated by the *osculating circle* at that point, an observation introduced for the geometry of co-circularity [**?**][1].

28.10 Summary

In summary, there are a number of different concepts behind co-circularity that we shall exploit in the next several chapters. The manner for selecting matches thus far has been relaxation labeling, but in subsequent chapter we shall also discuss how to use belief propagation and a more realistic reduction to neural circuitry. This latter reduction will require a re-interpretation of the relaxation labeling equations into the formal language of game theory.

- Geometric:
  - Approximate Curve in Local Neighborhood
    - Curvature $\Leftrightarrow$ Endstopping
  - Orientation Consistency Through Curvature
    - transport tangents $\Leftrightarrow$ projection fields

[1] Because of space limitations, references are very limited; we recommend that the original publications are consulted for additional references.

· Select "Optimal" Matches:

  – relaxation labeling ⇔ polymatrix games ⇔ network dynamics

